Degradable silyl–ether containing networks from tri-functional thiols and acrylates

*Caleb M. Bunton[1], Zahra M. Bassampour[1], Jennifer M. Boothby[2], Ashanti N. Smith[1], Joseph V. Rose[1], Daphne M. Nguyen[1], Taylor H. Ware[2], Karl G. Csaky[3], Alexander R. Lippert[1], Nicolay V. Tsarevsky[1], David Y. Son[1]**

[1]Department of Chemistry, Center for Drug Discovery, Design and Delivery (CD4), Southern Methodist University, Dallas, Texas

[2]Department of Bioengineering, The University of Texas at Dallas, Richardson, Texas. *Present affiliation:* Department of Biomedical Engineering, Department of Materials Science and Engineering, Texas A&M University, College Station, Texas

[3]Retina Foundation of the Southwest, Dallas, Texas

*Corresponding author: Professor David Y. Son, dson@smu.edu

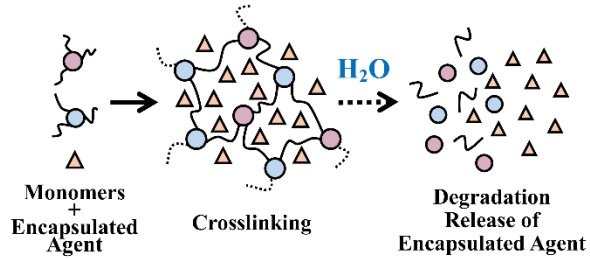

For Table of Contents use only

Abstract

The purpose of this study was the synthesis of novel degradable polymer-based devices capable of releasing an encapsulated agent in a controlled manner with specific interest for use as drug delivery materials. Base–catalyzed thiol–Michael additions between trithiols and triacrylates containing silyl ether groups were exploited to prepare a series of degradable crosslinked networks. Disodium fluorescein was loaded as a hydrophilic drug surrogate inside the networks, and the degradation of the networks and the release of dye were monitored. The networks were characterized by FTIR spectroscopy, and their thermal and mechanical properties were investigated through thermogravimetric analysis (TGA) and dynamic mechanical analysis (DMA). The effects of monomer structure on degradation, release behavior, and thermal properties were investigated. The networks prepared from more sterically hindered silyl ether monomers exhibited decreased rates of degradation and correspondingly slower release of encapsulated disodium fluorescein dye. The results suggest the characteristics of the networks can be fine–tuned by manipulation of the group attached to the Si atom in the silyl ether monomers.

Introduction

Hydrolytically degradable polymer networks are particularly attractive due to their potential applications in the biomedical field, including orthopedic implants, drug delivery, and scaffolds for tissue engineering.[1–5] These types of polymers can vary greatly in degradation rates (in some cases up to twelve–fold) for all different network formulations.[6] Currently used polymer systems of this nature include the hydrolytically unstable poly(α–hydroxy acids) such as poly(lactic acid) (PLA) and poly(lactic–co–glycolic acid) (PLGA), and the more hydrolytically stable bisphenol A (BPA) derived polycarbonates.[6,7] Other commonly utilized hydrolytically degradable polymers include short chain poly(α–esters), useful for regenerative purposes, such as tissue scaffolds, polyanhydrides used extensively in drug delivery applications, as well as polyurethanes in cardiac assist devices such as vascular shunts.[6] Drug delivery is one of the most significant applications of degradable

polymers.[6] High control over drug release kinetics is a primary factor to be considered for drug delivery systems. Also, polymers used for drug delivery should demonstrate ease of fabrication, lack of toxicity of both the staring materials and the products of their degradation, targeted delivery, and optimal release performance. Non–degradable networks may provide a sustained release either without an initial burst of release or with an initial burst of release if a loading dose is desired.[8,9] However, a secondary surgery may be required to remove the empty implant.[9] In this regard, degradable networks provide advantages through the ability to be implemented without the need for a secondary surgery for material removal.

PLA, PLGA, and polyglycolic acid (PGA) are examples of degradable polymers which have been used for various delivery purposes,[10] with lactic and glycolic acid as the degradation products. Release of compounds from these polymeric materials follows three steps: 1) initial burst release, 2) diffusive phase, and 3) final burst.[9] The initial burst release arises from the increased diffusivity of encapsulated compound on or near the surface of the material and is dependent on the material's surface area, encapsulated compound concentration within the material, and water solubility of the encapsulated compound. Pre–incubation with aqueous solvent for several hours to remove surface compound before use can overcome initial burst release. The diffusive phase is controlled by the polymer degradation rate, the total surface area of the material, the water solubility of the encapsulated compound, and its loaded concentration inside the network. An additional aspect of consideration, which may be exploited to enhance or diminish diffusive phase release through increased or decreased network degradation, is the pH of the environment where the network will be utilized.[11] Final burst release, which is a major disadvantage of degradable networks compared with their non–degradable counterparts, results from complete hydrolysis of polymer throughout the matrix during the diffusive phase. Final burst release is generally uncontrollable, unpredictable, and undesirable, and the higher ratio of volume to surface area increases its intensity. Networks comprised of polymers with differing molecular weights may address the unwanted final burst release. A polymer with a higher molecular weight usually degrades more slowly and can be applied as the framework, while a polymer with lower molecular weight may control the

release rate of the encapsulated compound due to faster degradation. Sustained release rates, comparable to those obtained from non–degradable materials, were observed from these types of networks.[12]

Silyl ethers, $(R'O)_nSiR_{4-n}$, are hydrolytically degradable groups that have been investigated recently by different research groups for the production of biocompatible materials.[13–17] The major hydrolysis products of the moisture sensitive Si–O bonds in silyl ethers are silanols, and alcohols, both of which are relatively non–toxic. The hydrolysis products also do not considerably change the pH of the surrounding environment. For these reasons, the hydrolytically labile silyl ether bonds are very promising for the production of degradable networks for biomedical applications.[13] The ability to control degradation rate through the attached groups on Si is another reason why applying silyl ethers as labile linkages in degradable network structures may be advantageous for drug delivery purposes.

Thiol–click chemistry has become increasingly used in polymer synthesis for biomedical applications such as drug delivery and cell targeting.[18] Polymeric materials obtained from thiol–click reactions should possess certain properties for drug delivery applications including non–toxicity and non–immunogenicity, the ability to target specific sites, and the ability to remain in the body long enough to achieve maximum therapeutic effect. All of these characteristics depend on the molecular architecture of the polymer as well as its functionality, which can be carefully controlled through thiol–click reactions.[2,18–27] The first example of the thiol–Michael addition reaction was reported in the 1960s by Allen et al.,[28] and since has become a critical tool for organic syntheses. Several research groups have exploited this reaction in polymer chemistry and material development.[20] While Michael addition reactions have historically been used in many organic syntheses, their application in polymer and material syntheses, as well as polymer modification, has become more prevalent in parallel to the broader implementation of click chemistry in material science.[25,27,29–32] The absence of a significant side product in both the nucleophilic and base catalyzed thiol–Michael addition reactions is a great advantage and is also the reason why thiol–Michael chemistry has become a chemistry of choice in many materials chemistry applications. Side reactions, such as the formation of radical–radical termination products formed in radical mediated thiol–ene reactions,[33,34] are absent in thiol–Michael reactions, even in very dilute

systems such as those necessary for polymer–polymer conjugation. Some applications of thiol–Michael reactions in materials chemistry include surface and particle modification, dendrimer synthesis, degradable hydrogel formation, and block copolymer synthesis.[35–38]

Utilizing the base–mediated thiol–Michael addition reaction, we have prepared novel silyl ether degradable implants capable of releasing an encapsulated agent in a controlled manner. A series of degradable crosslinked networks, loaded with disodium fluorescein dye as a drug surrogate, were produced and the degradation and release behavior of the networks were monitored. The effect of monomer structure on degradation, release behavior, and thermal properties was also investigated.

Experimental Section

Materials and Instrumentation. Monomers A3 and T3 are commercially available. Triethylamine was distilled from calcium hydride while the chlorosilane starting reagents were distilled from magnesium turnings prior to use. All organic solvents were dried over activated 4Å molecular sieves. The phosphate buffered saline (PBS) solution had a pH of 7.5.

NMR spectra were aquired with a JEOL 500 MHz NMR spectrometer, and chemical shifts are reported in parts per million (ppm) relative to $CDCl_3$ (δ 7.26) for ^1H NMR spectra, and (δ 77.2) for ^{13}C spectra. Network samples were divided to small pieces for obtaining ATR–FTIR spectra. Infrared spectra were aquired with the use of a Nicolet iS10 ATR–FTIR spectrometer (Thermo Scientific) with a ZnSe ATR crystal (Spectra–Tech). $LogP_{\frac{oct}{aq}}$ values were obtained using ACD/ChemSketch Freeware, version 2015.2.5. The onset of thermal decomposition temperature (T_d) was determined from thermal gravimetric analysis (TGA) using a SDT 2960 simultaneous DTA-TGA (TA Instruments). Samples with a mass between 6–7 mg were utilized for the TGA studies and were heated at a rate of 10 °C/min under N_2 (gas) flow. Glass transition temperatures (T_g) were reported from tan δ_{max} with dynamic mechanical analysis (DMA). Samples of each composition were cast in molds at 0.35 mm thickness and cut to 20 mm x 2 mm for testing. Samples for testing were stored in desiccated

containers for a maximum of two weeks. Immediately prior to testing, samples were incubated at 65 °C for one hour to evaporate any residual water. Samples were loaded into a TA Instruments RSA–G2 dynamic mechanical analyzer with a loading gap of 10 mm. Dynamic modulus was measured at 0.05% strain from -90 °C to 50 °C at a rate of 1.0 °C/min. The UV–Vis study was recorded on a SHIMADZU UV–VIS-NIR SPECTROPHOTOMETER UV–3600; absorbance data at 490 nm was used for dye release studies and amounts of dye released was calculated against a calibration curve created with standards between 5 and 50 μM.

Monomer synthesis. Monomers **A1**–**A2,** and **T1**–**T2** were synthesized using known methods.[14,39–42] To synthesize model compound **DG1**, 2–mercaptoethanol (3.3 g, 43 mmol) and 2–hydroxyethyl acrylate (4.9 g, 43 mmol) were mixed together, and 1–hexylamine (0.039 g, 0.38 mmol) was added as a catalyst. The reaction proceeded for 12 hours at room temperature, after which any unreacted starting materials were removed under reduced pressure (yield 90%). Although compound **DG1** is a known compound and has previously been synthesized in 50% yield, it was nonetheless missing important characterization data including detailed ^{1}H and ^{13}C NMR and data.[43] HETCOR and HMBC (2D NMR methods) were used to verify exact peak assignments (S.I., Figure S2). ^{1}H NMR (500 MHz, $CDCl_3$, δ): 4.20 (m, 2H, –OC*H*$_2$CH$_2$OH), 3.77 (m, 2H, –OCH$_2$C*H*$_2$OH), 3.70 (t, ^{3}J = 6.0, 2H, HOC*H*$_2$CH$_2$S–), 3.07 (s, 2H, O*H*), 2.79 (t, ^{3}J = 7.0, 2H, –SC*H*$_2$CH$_2$CO–), 2.69 (t, ^{3}J = 6.0, 2H, –C*H*$_2$O– or HOCH$_2$C*H*$_2$S–), 2.63 (t, ^{3}J = 7.0, 2H, C*H*$_2$O or HOCH$_2$C*H*$_2$S-). ^{13}C NMR (125 MHz, $CDCl_3$, δ): 172.4 (CO), 66.3 (HOCH$_2$*C*H$_2$O-), 60.9 (HO*C*H$_2$CH$_2$S–), 60.8 (HO*C*H$_2$CH$_2$O–), 35.2 (HO*C*H$_2$CH$_2$O–), 34.9 (–SCH$_2$*C*H$_2$CO– or –S*C*H$_2$CH$_2$OH), 26.9 (–S*C*H$_2$CH$_2$CO).

Network Synthesis. For the preparation of networks **XL1**–**7**, the appropriate thiol and acrylate monomers were mixed in a 1:1 mole ratio of SH:acrylate. In dye containing networks, disodium fluorescein (1 % (*w/w*)) was added to the monomer mixture and the dispersion was stirred vigorously with a glass stirring rod for 2-3 minutes. The mixture was then placed into a sonicator for five minutes to ensure dye/monomer mixture homogeneity. The 1–hexylamine (270:1 mole ratio alkene/thiol:amine) catalyst (as a 1 M solution in THF) was then added to the monomer mixture. The mixture was stirred vigorously for 30 seconds with a glass stirring rod

and poured into individual, cylindrical HDPE plastic molds. Cylindrical HDPE plastic molds with an average diameter of 1.2 cm and height of 1.3 cm were utilized to produce consistently sized samples. Samples were cured for one hour at room temperature in their respective cylindrical HDPE molds followed by a one–hour post–cure at 160 °C, or a 1.5–hour room temperature cure followed by a 2–hour post–cure at 70 °C. Network samples with an average mass of 0.50 g were prepared by the following methods:

XL1 was prepared by mixing monomer **T1** (0.21 g, 0.76 mmol) with monomer **A1** (0.29 g, 0.76 mmol) and 1–hexylamine (1.7 mg, 16.9 μmol) catalyst. ATR–FTIR **XL1** (neat) υ (cm^{-1}): 773 (m), 962 (m), 1070 (s), 1265 (w), 1408 (w), 1729 (s), 2914 (m).

XL2 was prepared by mixing monomer **T2** (0.23 g, 0.69 mmol) with monomer **A1** (0.27 g, 0.69 mmol) and 1–hexylamine (1.7 mg, 16.9 μmol) catalyst. ATR–FTIR **XL2** (neat) υ (cm^{-1}): 699 (m), 737 (m), 810 (w), 1073 (s), 1251 (w), 1429 (w), 1730 (s), 2916 (m), 3020 (w).

XL3 was prepared by mixing monomer **T2** (0.21 g, 0.63 mmol) with monomer **A2** (0.29 g, 0.63 mmol) and 1–hexylamine (1.7 mg, 16.9 μmol) catalyst. ATR–FTIR **XL3** (neat) υ (cm^{-1}): 697 (m), 737 (m), 1073 (s), 1244 (w), 1429 (w), 1728 (s), 2916 (m), 3050 (w).

XL4 was prepared by mixing monomer **T3** (0.29 g, 0.71 mmol) with monomer **A3** (0.21 g, 0.71 mmol) and 1–hexylamine (1.7 mg, 16.9 μmol) catalyst. ATR–FTIR **XL4** (neat) υ (cm^{-1}): 780 (w), 1016 (w), 1131 (s), 1349 (m), 1540 (w), 1727 (s), 2917 (m).

XL5 was prepared by mixing monomer **T3** (0.072 g, 0.18 mmol), monomer **A3** (0.053 g, 0.18 mmol), monomer **T1** (0.16 g, 0.56 mmol), and monomer **A1** (0.22 g, 0.56 mmol) and 1–hexylamine (1.7 mg, 16.9 μmol) catalyst. ATR–FTIR **XL5** (neat) υ (cm^{-1}): 777 (m), 964 (m), 1030 (w), 1077 (s), 1240 (w), 1347 (m), 1378 (m), 1728 (s), 2918 (m).

XL6 was prepared by mixing monomer **T3** (0.14 g, 0.36 mmol), monomer **A3** (0.10 g, 0.36 mmol), monomer **T1** (0.10 g, 0.38 mmol), and monomer **A1** (0.14 g, 0.38 mmol) and 1–hexylamine (1.7 mg, 16.9 μmol) catalyst. ATR–FTIR **XL6** (neat) υ (cm^{-1}): 776 (m), 964 (m), 1078 (m), 1131 (m), 1347 (m), 1727 (s), 2917 (m).

XL7 was prepared by mixing monomer **T3** (0.21 g, 0.54 mmol), monomer **A3** (0.16 g, 0.54), monomer **T1** (0.052 g, 0.19 mmol), and monomer **A1** (0.072 g, 0.19 mmol) and 1–hexylamine (1.7 mg, 16.9 μmol) catalyst. ATR–FTIR **XL7** (neat) υ (cm^{-1}): 780 (m), 979 (w), 1077 (w), 1128 (m), 1348 (m), 1463 (m), 1726 (s), 2964 (m).

ATR–FTIR spectra may be found in the supplemental information (Figure S1)

Degradation and Release Studies. The dry masses (m_d) of the **XL** samples were recorded prior to conducting degradation studies. Each **XL** sample was immersed in 10 mL of PBS and kept at 37 °C. Mass change was monitored over a period of 30 days by removing each sample from the PBS, gently drying the sample surface with an absorbent wipe, and recording its wet mass (m_w). To determine the exact amount of loaded dye inside each **XL** sample, the molds in which the samples were prepared were immersed in 10 mL of PBS. Solution absorbances at λ_{max}=490 nm was then obtained via UV spectroscopy and their concentrations were calculated against a calibration curve of known concentrations. The calculated amount of dye in each solution was then subtracted from the original amount of loaded dye. After each mass measurement, the **XL** samples were placed into fresh PBS and the old solutions were used to calculate the amount of dye released using UV spectroscopy

Degradation Product Analysis. XL samples without dye were prepared and immersed in PBS for 30 days in order to ascertain the degradation product. The aqueous layer of the solutions containing the degradation product was extracted using deuterated–chloroform ($CDCl_3$), and the organic layer was then analyzed using multinuclear (^1H and ^{13}C) NMR spectroscopy and GC–MS. The model degradation compound, compound **DG1**, was synthesized as described previously and characterized using similar methods. To confirm the

structure of the degradation product, the spectra and chromatogram data of the degradation product were compared to the results obtained from the model compound.

MTT Assays for Toxicity. Human lung adenocarcinoma epithelial cells (A549) were purchased from ATCC and cultured in Ham's F–12K (Kaighn's) media supplemented with 10% fetal bovine serum (FBS) and 1% antibiotics (penicillin/streptomycin, 100 U/mL). Cells were maintained in a humidified incubator at 37 °C with 5% CO_2. One day before the assay, cells were passaged and seeded in a 96–well plate to a total of 205 μL/well. The plate was incubated at 37 °C with 5% CO_2 for 18 hours. The media was then removed when 70–80% confluency was reached, and the cells were washed with PBS phosphate buffer. The thiol–acrylate degradation product (**DG1**) was added at 0, 0.05, 0.5, 5, and 50 mM respectively in 100 μL of complete F–12K media, followed by incubation for another 20 hours. 10 μL of the MTT reagent (Cayman Chemical, Ann Arbor, MI) was then added to each well and mixed gently. After 3 hours of incubation, 100 μL of crystal dissolving solution was added to each well to dissolve the formazan crystals that had formed. Absorbance was recorded the next day in a Cytation 5 BioTek plate reader at 570 nm. Cell viability was expressed as a ratio of the control. Experiments were accomplished with 6 technical replicates and 2 biological replicates.

Results and Discussion

Monomer synthesis and optimization of cure conditions. Silyl ether–containing acrylates and thiols were synthesized through substitution reactions of methyltrichlorosilane and phenyltrichlorosilane (Scheme 1).[14,39–42]

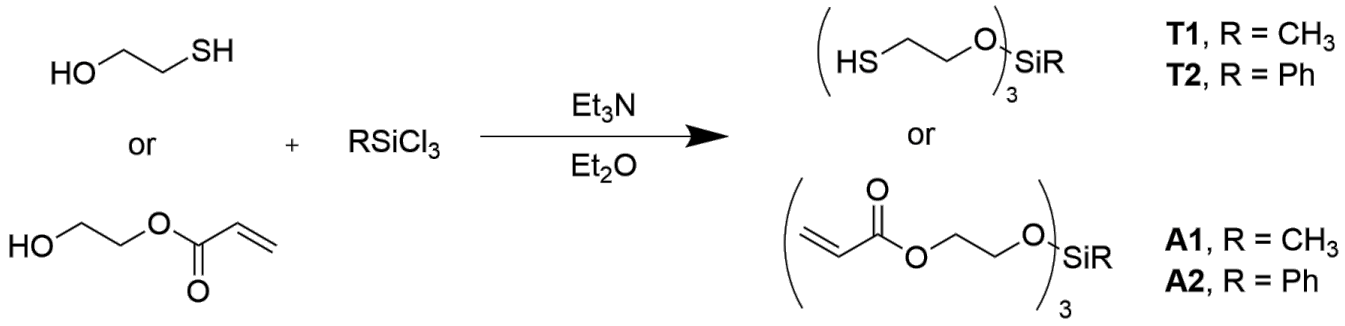

Scheme 1: Synthesis of silyl ether monomers.

Monomers for this study were selected that possess the same number of functional groups (three), but with either a methyl or phenyl group attached to the Si atom. The presence of hydrolyzable Si–O bonds gives degradable characteristics to the networks, and the different R groups affect water accessibility to the degradable bonds. Commercially available tri–thiol **T3** and tri–acrylate **A3** (Figure 1) were also included in this study to prepare networks that possess only conventional ester linkages.

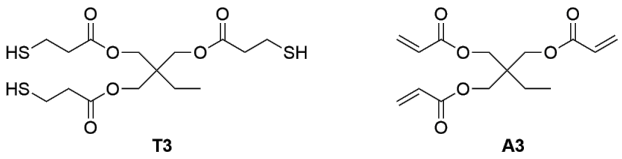

Figure 1. Commercially available monomers employed in this study.

This allows for comparisons to be made with the networks containing more sensitive silyl ether bonds. The general crosslinking scheme and degradation process are summarized in Scheme 2).

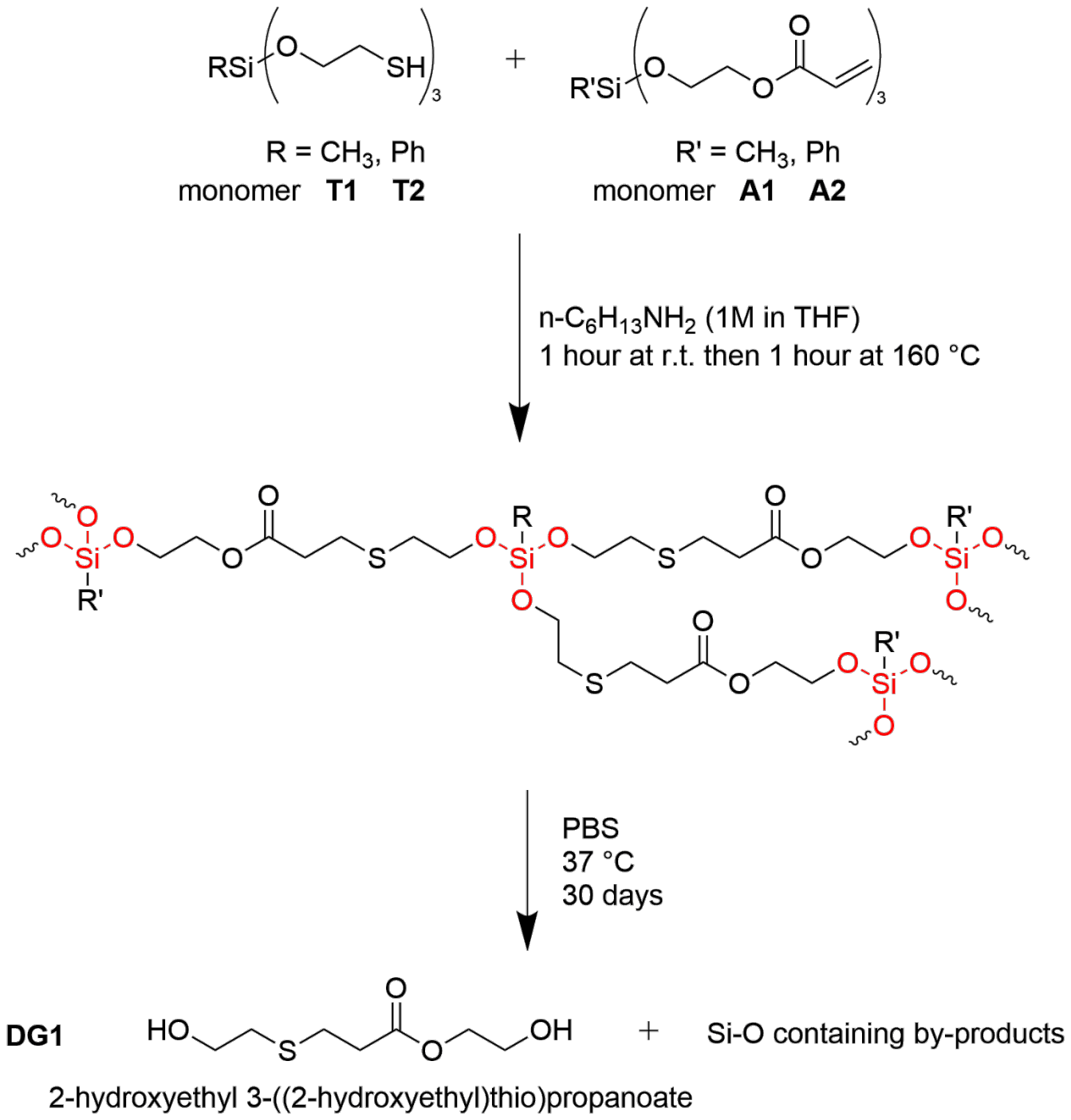

Scheme 2. Schematic of network structures and degradation product **DG1**.

In order to determine the optimal catalyst concentration, solutions of 1–hexylamine in THF were prepared at 0.5, 1, and 3 M concentrations. Neat 1–hexylamine was also studied. The onset of crosslinking and its progress were monitored both visually and by physical inspection in the network samples prepared from different amounts of catalyst over 24 hours. Based on our observations, a 1 M solution of 1–hexylamine (270:1

mole ratio alkene/thiol:amine) was determined to be the optimal catalyst solution. Working with this catalyst solution allowed us to thoroughly mix the network ingredients before crosslinking started, resulting in homogeneously cured networks.

Optimized cure conditions ensure maximum monomer conversion is achieved. Maximum monomer conversion also decreases the possibility of unreacted or partially reacted monomers leaching out of the crosslinked materials. For this reason, mixtures of monomers were prepared under various curing temperature conditions. The cured networks were then allowed to soak in acetone or THF overnight, followed by a 12–hour drying period. The difference between the original mass of each network and its mass after the 12–hour drying period was considered as the mass of the uncrosslinked portion of the networks. Network samples prepared using a one hour room temperature cure, followed by a one hour post cure at 160 °C, did not exhibit more than a 2% mass loss. To further confirm completion of cure, ATR-FTIR spectra of all networks indicated complete loss of the S–H absorbance (~2570 cm^{-1}, Figure S1). As a result, the conditions described above were used for curing the networks described in this study.

The Effect of R–Si Groups on Network Degradation Behavior. Various crosslinked networks were produced using silyl ether acrylates (**A1** and **A2**) and silyl ether thiols (**T1** and **T2**) containing either methyl groups (**XL1**), phenyl groups (**XL3**) or a mixture of both (**XL2**; **T1** + **A2**) attached to the Si atom, Figure 2. To exclusively explore the effect of the R group on network degradation and release behavior, and exclude the effect of crosslink density, starting materials were selected that possessed the same degree of functionality (three). To compare the degradation and release behavior of silyl ether networks to those containing only ester linkages, network **XL4** was prepared from commercially available monomers **T3** and **A3**. No hydrolyzable Si–O bonds are present in **XL4**, whereas the other networks (**XL1–3**) possess hydrolyzable silyl ether bonds.

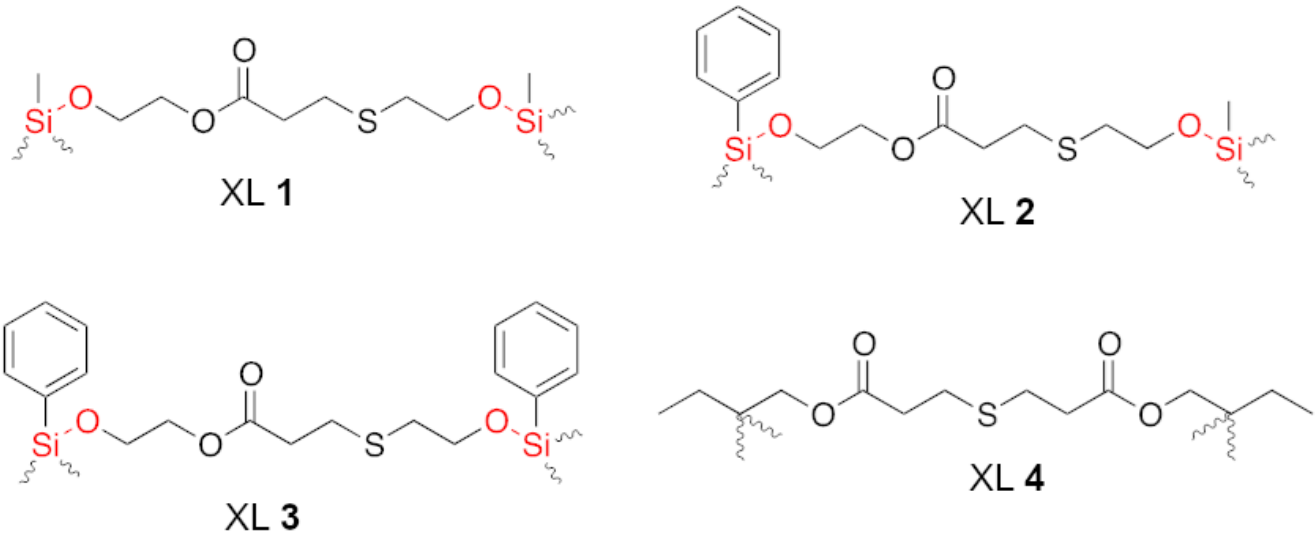

Figure 2. Networks synthesized in this study.

In comparison to methyl groups, phenyl groups are responsible for increasing steric hindrance and hydrophobicity towards the chemical environment around the silyl ether linkages. In order to gain insight into the hydrophobic/hydrophilic nature of the monomers, and the ability of their corresponding networks to readily undergo hydrolytic degradation, a partition coefficient (*Log*P) was calculated for each monomer. The partition coefficient (P) describes the ability of the monomers to dissolve in the water portion vs. organic portion of a biphasic system such as water and octan–1–ol (Equation 1).[44,45]

Equation 1: $$LogP_{\frac{oct}{aq}} = Log\frac{[Monomer_{oct}]}{[Monomer_{aq}]}$$

The $LogP_{\frac{oct}{aq}}$ values for monomers can be acquired through experimental measurements. However, due to the hydrolytic sensitivity of the monomers in this study, leading to decomposition during data collection and a skewing of the results, a calculation method was utilized to obtain $LogP_{\frac{oct}{aq}}$ values with greater accuracy. The *Log*P$_{oct}$ values for the monomers were obtained from ACD/ChemSketch Freeware, version 2015.2.5. (Table 1).[45] ACD/ChemSketch Freeware uses a mixed atom/fragment constructionist structure approach and is

reported to be a reliable source for predicting $LogP_{\frac{oct}{aq}}$ values.[45] Based on the $LogP_{\frac{oct}{aq}}$ values of the monomers, the hydrophobicity of the networks were expected to increase from **XL1** to **XL3**.

Table 1: $LogP_{\frac{oct}{aq}}$ values calculated from ACD/Labs.

Monomer	Calculated $LogP_{\frac{oct}{aq}}$
T1	2.21 ± 0.57
A1	2.79 ± 0.56
T2	3.47 ± 0.40
A2	4.05 ± 0.38
T3	3.02 ± 0.48
A3	1.50 ± 0.38

Once the networks were prepared, samples were soaked in phosphate–buffered saline (PBS) solution with pH of 7.4 at 37 °C for a maximum of 30 days, and the mass change (%) during that time was determined by measuring the difference between the soaked sample mass and the original mass.

The wet mass was measured after the sample was patted dry with an absorbent wipe. Samples of **XL1**–**3** exhibited slight increases in mass (2.5–3.0 wt%) during the first few days, indicating the penetration of aqueous PBS solution at the beginning of the degradation process. To ascertain if any degradation product was released while the networks were gaining mass, fresh samples of **XL1**–**3** were allowed to soak in D_2O. NMR spectroscopic analyses of the solutions were performed after one, three, and six hours, and after one day. The NMR spectra revealed the presence of degradation product released from **XL1**–**3** from the first measurement, after one hour of soaking in D_2O (NMR data reported below). The amount of degradation product released was found to increase over time. This observation confirmed that although the **XL1**–**3** networks did not show any significant mass loss within the first few days, release of the degradation product occurred almost immediately after the networks were exposed to the aqueous solution. Mass loss data over time for networks **XL1**–**4** are shown in Figure 3.

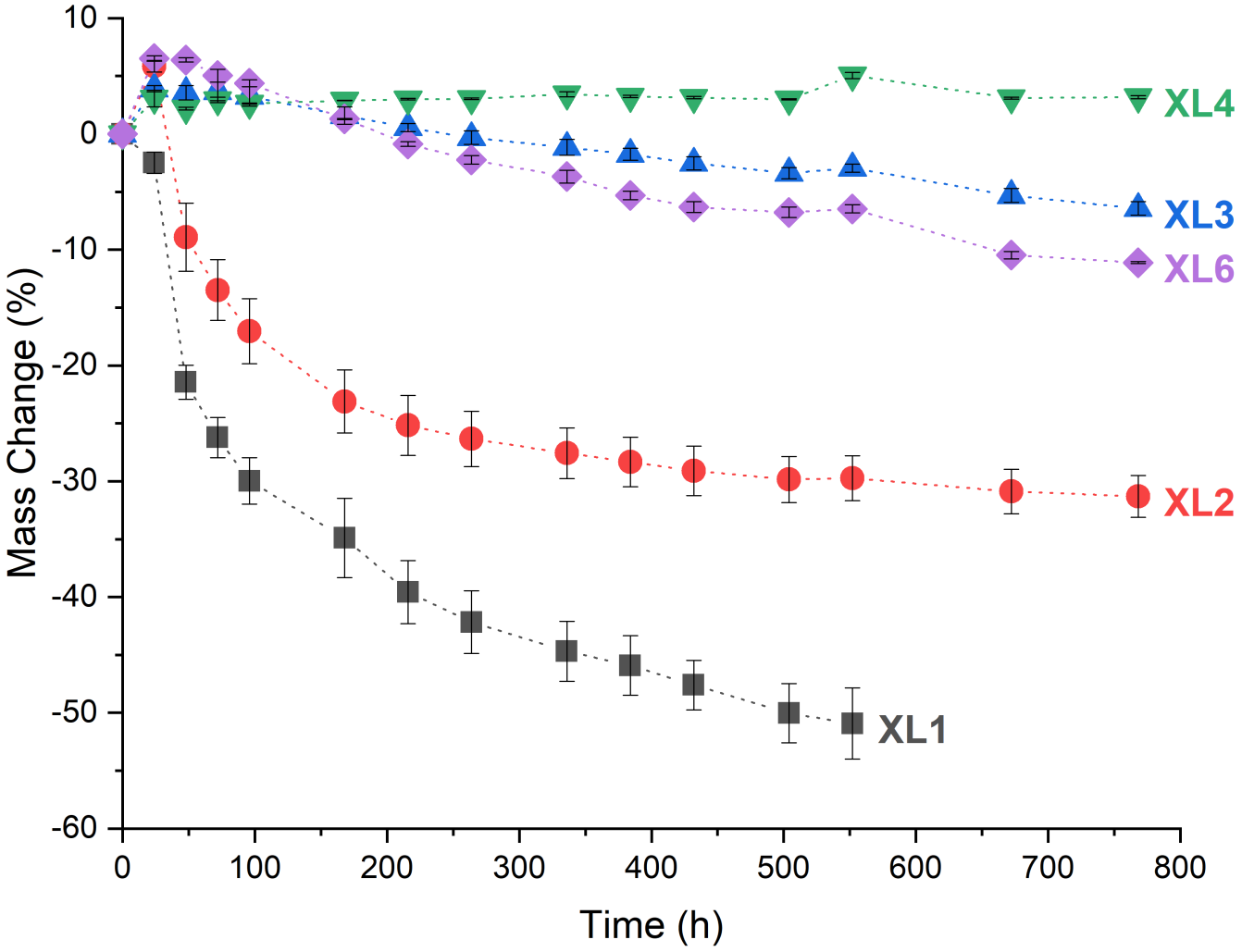

Figure 3. Degradation of **XL1**–**4** and **XL6** (as described below) in PBS at 37 °C.

Monitoring the mass changes of **XL1**–**4** revealed that the greatest mass loss overall (–51 wt%) was obtained for **XL1**. The monomers utilized for the preparation of **XL1** possess a sterically small methyl group attached to the Si atom, as well as the lowest value of $LogP_{\frac{oct}{aq}}$ (lowest hydrophobicity), compared to the other silyl ether monomers utilized in this study. The reduced steric hindrance around the hydrolyzable bonds and the greater water accessibility in **XL1** can explain the larger mass loss observed for this network. The second highest mass loss (–31 wt%) was observed for **XL2**. The decreased degradation of **XL2** compared to **XL1** was due to replacing thiol **T1** with the more sterically hindered and hydrophobic phenyl–containing thiol **T2**. Increased steric hindrance and hydrophobicity decreases the diffusion of water into the network and therefore results in decreased degradation. The reduction in degradation became more significant in **XL3** (–6 wt%), in

which both monomers have phenyl groups and relatively large $LogP_{\frac{oct}{aq}}$ values. A mass gain of 5 wt% without any evidence of mass loss or degradation was observed for **XL4**. The absence of degradation in **XL4** confirms the increased susceptibility of silyl ether bonds toward hydrolytic degradation, especially when compared to ester linkages. This was also useful to confirm that the mass loss observed from **XL1–3** was mainly due to the cleavage of the silyl ether bonds.

In order to investigate the possibility of further tuning degradation behavior, equal mole quantities of monomers **A1**, **A3**, **T1**, and **T3** were mixed to produce a new network, **XL6.** Monomers **T1** and **T3**, and **A1** and **A3** were utilized previously in the preparation of **XL1** and **XL4**, so a network prepared by mixing these four monomers was expected to possess intermediate degradable characteristics. The addition of the "non–degradable" monomers (**T3** and **A3**) should decrease the degradability of the resulting network. A representative structure of the resulting network is shown in Figure 4.

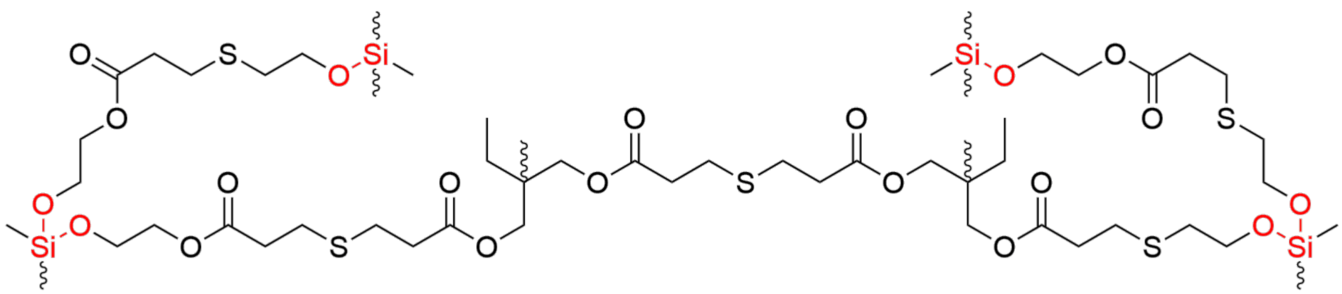

XL**6**

Figure 4: Mixed network **XL6**, produced by mixing monomers **T1** and **T3**, with **A1** and **A3**.

Samples of **XL6** in PBS at 37 °C exhibited a maximum swelling mass of 6.5 wt%. The onset of mass loss for **XL6** was observed on the second day. The mass changes observed for **XL6** were intermediate to the changes observed for both **XL2** and **XL3** over a 30–day period**.** The trend in the degradation profile of network **XL6** leads to the conclusion that the degradation rate of thiol–acrylate networks may be carefully tuned through the precise combination of thiol and acrylate monomers.

Effect of Silyl R Groups on Dye Release. For this study, a 1.0 % (*w/w*) mass of disodium fluorescein salt was loaded in all the synthesized networks. The dye is water-soluble and was used as a hydrophilic drug model.[46] Crosslink density,[47] degradation,[48,49] and diffusion[50] are three factors that control the release of an encapsulated agent from its host system. In this study, the effect of crosslink density was partially excluded by selecting monomers that possess the same degree of functionality. The effects of the two remaining factors were studied by measuring the UV absorbance of aqueous PBS solutions containing the dye–loaded networks over 30 days and calculating released dye percentages.

By monitoring the release of dye from the networks (Figure 5), a strong correlative relationship between network degradation and dye release was demonstrated. As the networks degraded, encapsulated dye was released to the surrounding medium. The fastest dye release was observed from network **XL1**, which also possessed the highest rate of degradation. Slower dye release from networks **XL2** and **XL3**, compared to **XL1**, corresponded to the observed slower degradation. It was found that **XL2** released the encapsulated dye faster than **XL3** with 63 % total mass of dye released from **XL2**, compared to 48 % from **XL3** over a 30–day monitoring period. A burst release of dye at the very beginning of the measurement period, when the amount of degradation based on mass change measurements was negligible, suggests that diffusion, which is related to the void size in the networks and the degree of interaction of the dye with the polymer, could be another contributing factor affecting the release of the encapsulated dye from the networks. The lowest amount of released dye (17 %) was observed from network **XL4**, which did not show any significant mass loss over a 30–day monitoring period. This observation confirms a contributing role of diffusion towards the release of dye from the networks, but that it plays a minor role towards release when compared to degradation. Therefore, for slower release rates, the incorporation of monomers **T3** and **A3** may be essential.

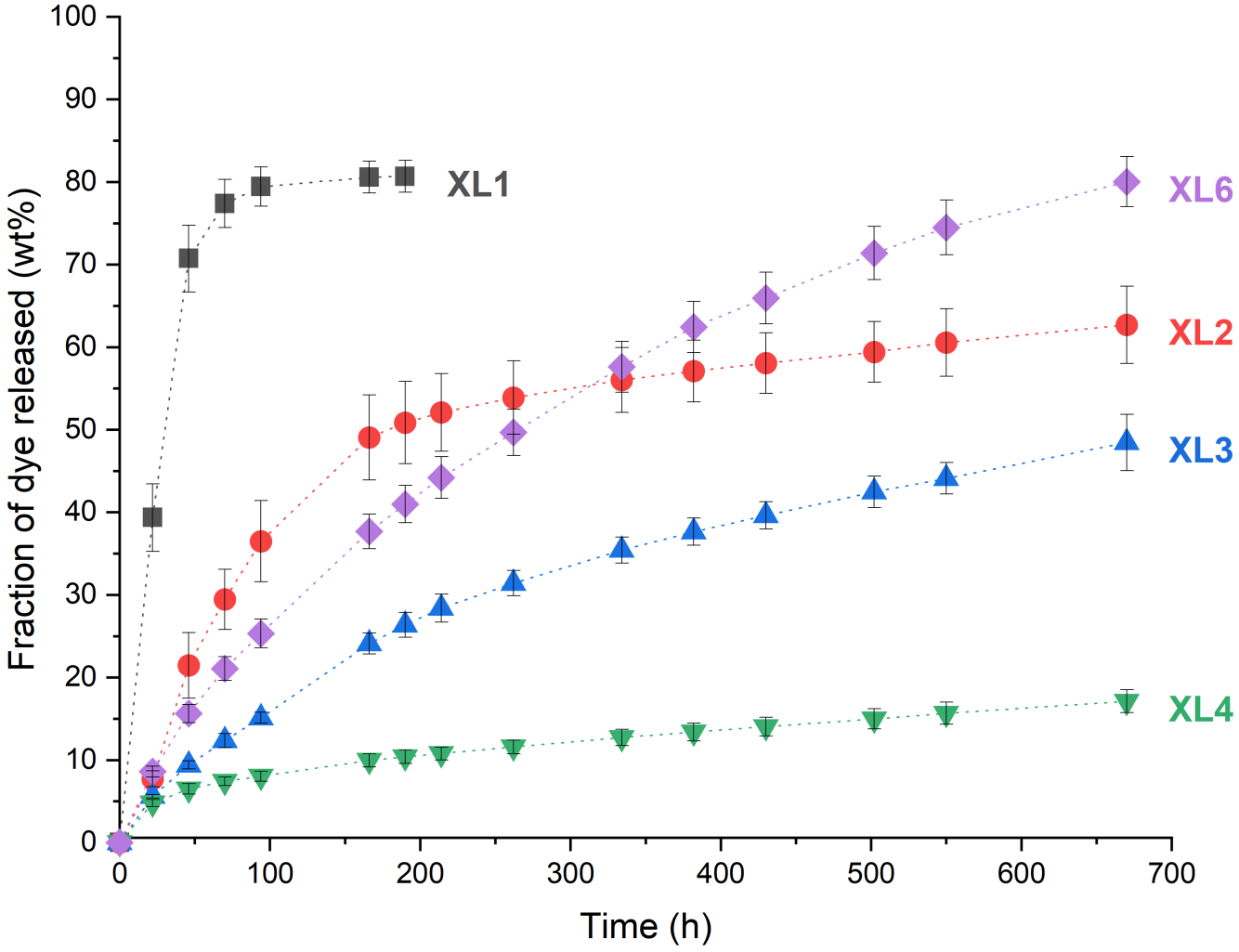

Figure 5. Disodium fluorescein dye release from **XL1**–**4**, and **XL6** in PBS at 37 °C. Fraction of dye released (wt%) obtained by taking solution absorbances via UV spectroscopy at λ_{max}=490 nm. Concentrations were calculated against a calibration curve of solutions of known concentration.

The release behavior of the dye-loaded **XL6** network, prepared from an equal combination of monomers **T1**, **T3**, **A1**, and **A3**, was monitored over 30 days (Figure 5) to investigate the possibility of further tuning release behavior. The release behavior of **XL6** agreed with the degradation behavior observed from networks **XL1** and **XL4**; faster dye release was found for the more degradable networks. The release behavior of **XL6** however, did not exactly parallel its degradation behavior as seen by **XL6** releasing more dye than **XL2**, while degrading to a lesser extent than **XL2**. This interesting behavior is almost certainly caused by the non-

degradable portions of the **XL6** network remaining intact within the network but still able to release dye. As the degradable portions of **XL6** hydrolyze, the surface area of the local domains of non-degradable network portions increases, which contributes to the increased diffusive release of dye from the network. A total mass % dye release of 80% was observed with **XL6**.

In summation, the degradation and consequent release process result from a balance between steric hindrance and hydrophobicity of the local environment surrounding the Si center of each monomer. Depending on the balance of those factors, cleavage of Si–O bonds can occur at different rates. This is evident when comparing degradation (Figure 3) and release (Figure 5) characteristics for each network, where networks containing an increase in methyl–Si functionality both degrade and release the encapsulated agent through hydrolytic diffusion more readily than networks containing a greater amount of phenyl–Si functionality.

Characterization of the Degradation Product. Samples of **XL1**–**3** were prepared and soaked for 30 days in PBS at 37°C, and their degradation products were identified using ^{1}H and ^{13}C NMR spectroscopy as well as GC–MS (Figure 6, Figure S2–S4). Samples for NMR spectroscopy were obtained by extracting the degradation product from the aqueous layer with $CDCl_3$. The expected degradation product 2–hydroxyethyl–3–((2–hydroxyethyl)thio)propanoate (**DG1**), was synthesized through a thiol–Michael addition reaction between 2–hydroxyethyl acrylate and 2–mercaptoethanol (Scheme 3).[43] In the networks, **DG1** is released by hydrolytic cleavage of the two Si–O bonds that connect the compound to the rest of the network structure (Scheme 2).

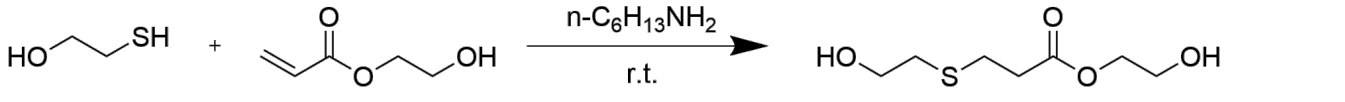

DG1
2-hydroxyethyl 3-((2-hydroxyethyl)thio)propanoate

Scheme 3: Synthesis of the degradation product, **DG1**.

The spectra and chromatograms obtained from the degradation product were compared to those obtained for the expected degradation product **DG1**, prepared separately (Scheme 3). Exact peak assignments were

verified via 2D NMR techniques including HETCOR and HMBC (Figure S4). The cleavage of Si–O bonds in the network resulting in the formation of degradation product **DG1** was confirmed (Scheme 2). The only discrepancy between the ^{1}H NMR spectra of the degradation product and that of **DG1** is the location of the OH peaks; the fluctuation of the hydroxyl protons in various chemical environments has been previously reported.[14]

Based on the similarity of the NMR spectra of the degradation product from the network samples and model compound **DG1**, we concluded that the compounds are the same.. (Figure 6).

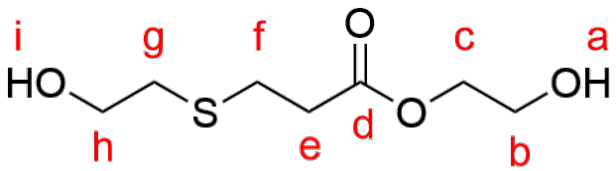

DG1

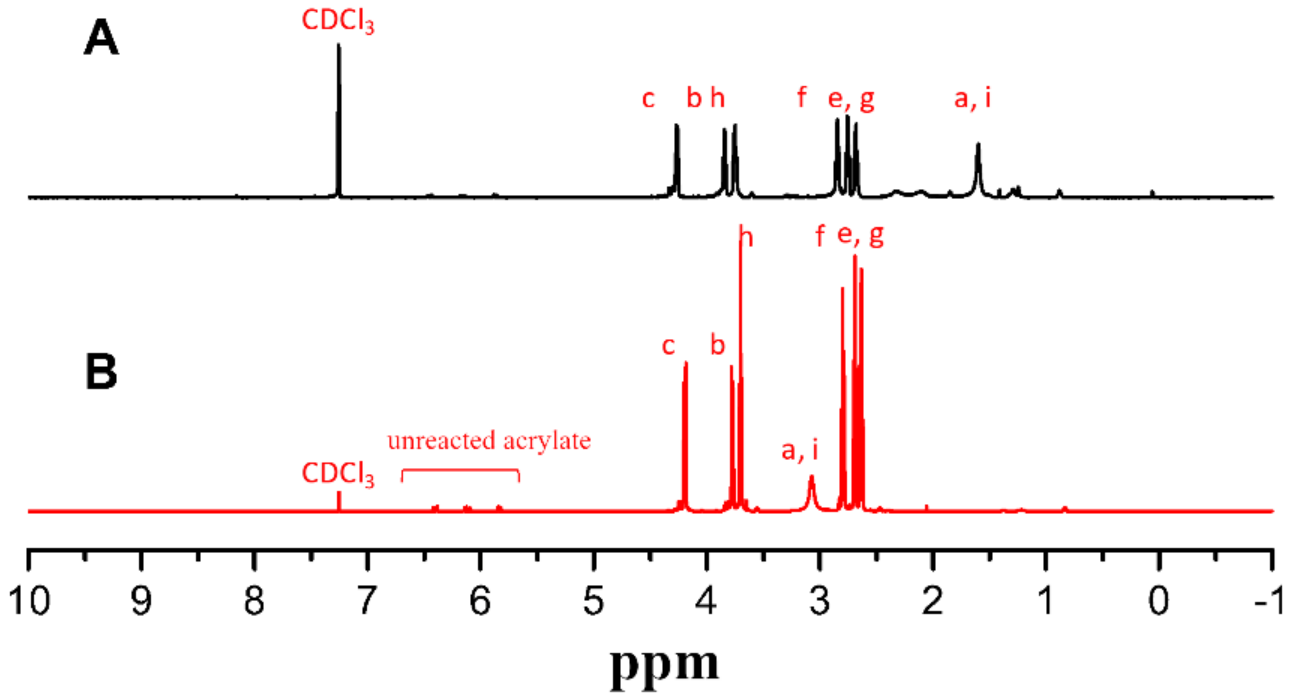

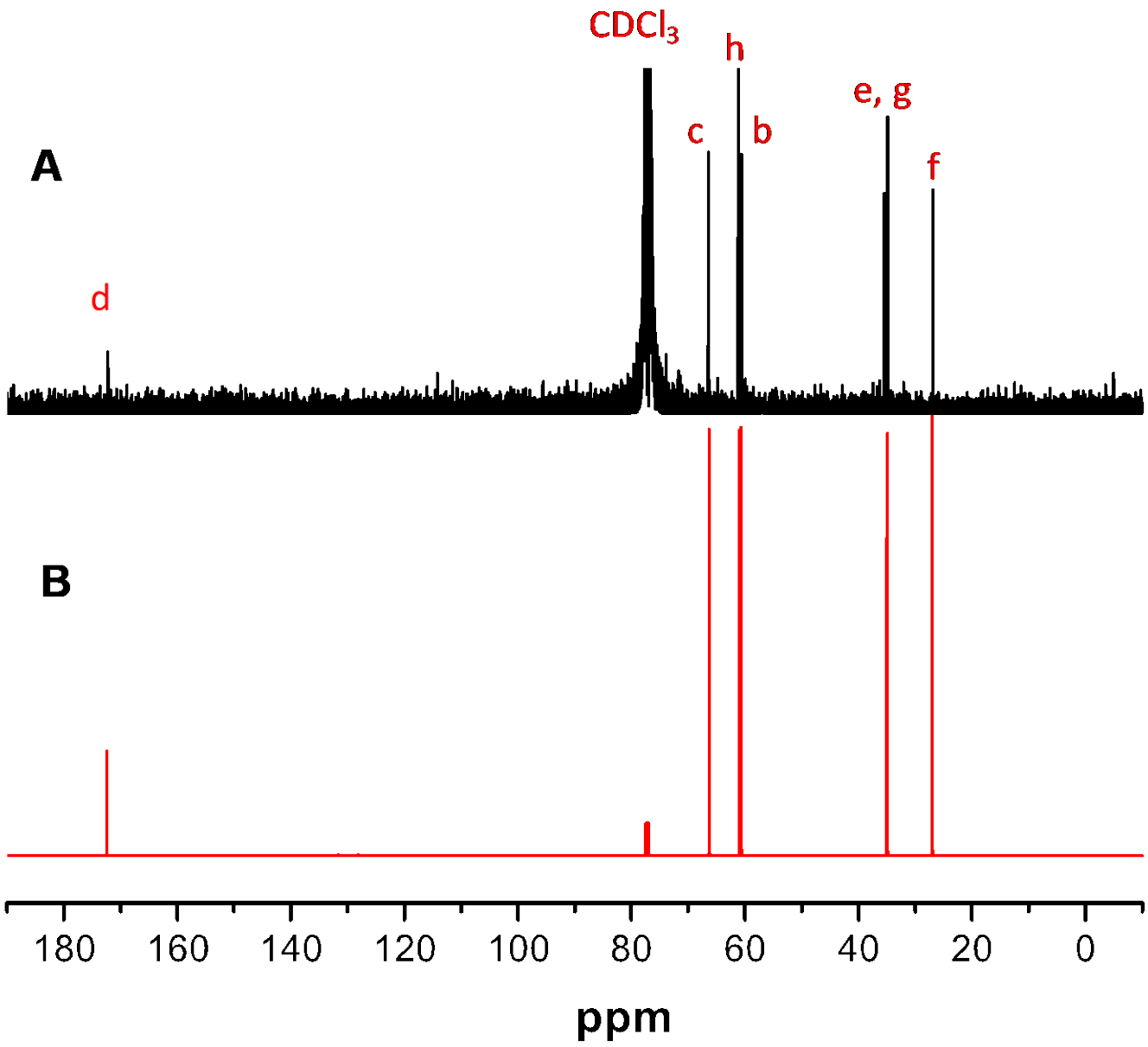

Figure 6. ^{1}H (top) and ^{13}C NMR (bottom) spectra of the degradation product from networks **XL1–3** in PBS at 37 °C (A), and model compound **DG1** (B), which was synthesized from the addition reaction of 2–mercaptoethanol and 2–hydroxyethyl acrylate.

Toxicity of the Degradation Product. A toxicity study of the degradation product (**DG1**) was accomplished with the use of MTT assays using human lung adenocarcinoma epithelial cells (A549). During the study, cells take up 3–(4,5–dimethylthiazol–2–yl)–2,5–diphenyltetrazolium bromide (MTT), a positively charged tetrazole compound with a yellow color. Due to its positive charge it passes through the negatively charged cell membrane. Intracellular enzymes in living cells called NAD(P) oxidoreductases reduce MTT to

formazan, which is characterized by a dark purple color. Without the enzymes (i.e., in dead cells) the cell growth media remains yellow.[51]

Through the MTT assays, it was found that the degradation product (**DG1**) did not cause a significant reduction of cell metabolic activity at all concentrations below 50 mM, the highest concentration. At 50 mM degradation product (**DG1**) concentration, cell viability was reduced to approximately 60% (Figure 7).

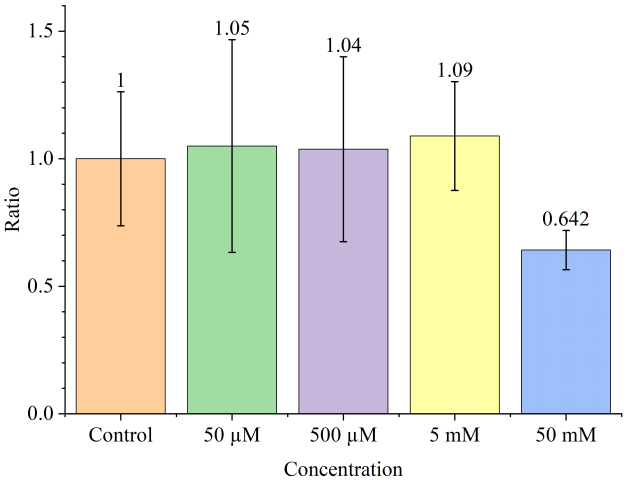

Figure 7: Toxicity study using network degradation product (**DG1**), $p < 0.05$.

A survey of published studies on polymer toxicity reveals that it is generally low, except in cases where pendant or easily accessible backbone functionalities are present, which themselves possess biological activity or toxicity, e.g., cationic (ammonium or pyridinium) groups, which are known as potent biocides. Typically, the toxicity associated with most polymeric materials is due to the presence of residual monomer, solvent, initiator, and/or catalyst used in the synthesis, plasticizers or other additives, and/or the release of bioactive compounds upon degradation.[52] This is why, in the present study, we have concentrated on examining the toxicity of the products of hydrolytic degradation of the networks, which are most likely to be released in real-life applications. In addition, we did not examine the toxicity of the amine catalyst due to its presence in extremely low concentrations.

Thermal Characterization. Thermal characterization of the networks, and especially understanding the glass transition temperature (T_g) of the networks, are important for some biomedical applications; T_g can profoundly influence the appropriateness of networks for a given application. For example, if the networks are to be useful as medical implants or contact lens–type devices, a softening of the network may be desired when subjected to biological conditions.[14] Thermal characterization of all the networks was performed using TGA and DMA. In addition to the previously described mixed network **XL6**, two additional mixed networks were prepared for thermomechanical characterization (Table 2).

Table 2. Formulations utilized for the preparation of **XL5** and **XL7**, with **XL6** shown for comparison.

	mol% Present (of total)			
Network	Monomer **T3**	Monomer **A3**	Monomer **T1**	Monomer **A1**
XL5	12.5	12.5	37.5	37.5
XL6	25	25	25	25
XL7	37.5	37.5	12.5	12.5

TGA measurements were conducted to determine the thermal stability of **XL1**–**7**. All the networks exhibited approximately the same onset of thermal decomposition temperature (T_d) of about 310 °C via a single step mechanism (Figure 8). Networks were found to possess char yields between 12–22% for the **XL1**–**XL4** networks, and 2–12% for the mixed **XL5**–**XL7** networks.

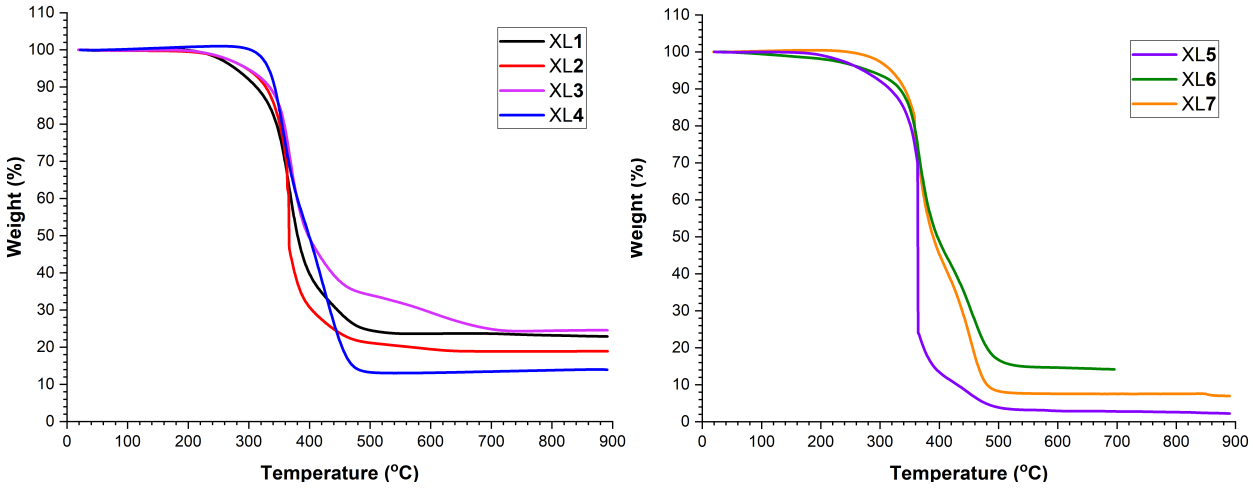

Figure 8. Thermal gravimetric analysis results for **XL1**–**7**; heating rate 10 °C/min; N_2 atmosphere.

Dynamic mechanical analysis (DMA) was used to determine the storage modulus as a function of temperature and glass transition temperature (T_g). First, the properties of **XL1**–**XL4** were compared (Figure 9, **A**–**B** and Table 3). All compositions were found to possess a similar glassy modulus, but the rubbery modulus is lower in compositions containing silyl ether bonds. The highest glass transition from all formulations was the control sample **XL4** (T_g = –2.3 °C), as compared to the silyl ether containing network samples **XL1** (T_g = –48.2 °C), **XL2** (T_g = –38.3 °C), and **XL3** (T_g = –39.5 °C) all of which have lower glass transitions due to the presence of flexible silicon–oxygen bonds. It was expected that the glass transition temperatures would increase as the concentration of phenyl groups increased. Indeed, **XL2** had a higher glass transition as compared to **XL1**; however, **XL3** had a similar glass transition temperature instead of the expected increased transition. This could be due to the relatively lower reactivity of the monomer containing two phenyl groups, which may result in a slightly lower crosslink density in this composition than in the other compositions. This is also evidenced in the slightly lower glassy modulus and lower rubbery modulus as compared to the other samples. As the silyl ether and non–degradable monomers are mixed in varying quantities, the glassy moduli of the networks (**XL5**–**7**) remain relatively the same (Figure 9, **C**). The glass transition temperature trends as expected between the mixed polymer compositions of **XL5** (T_g –34.4 °C), **XL6** (T_g –22.5 °C), and **XL7** (T_g –14.8 °C) with decreasing silyl ether content trending towards higher glass transition (Figure 9, **D**).

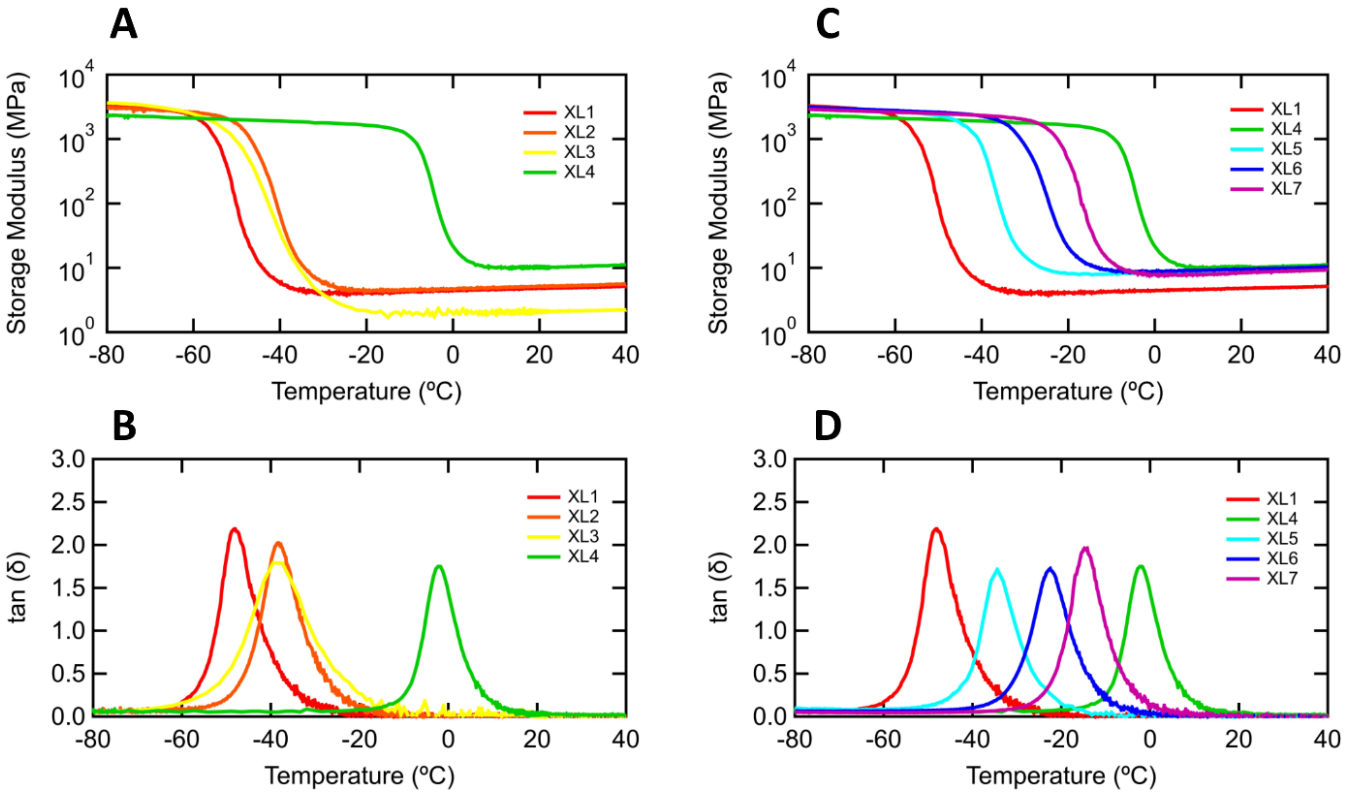

Figure 9. Dynamic mechanical analysis results for **XL1–7**; 0.05% strain from –90 °C to 50 °C at a rate of 1.0 °C/min.

Table 3. Summary of thermal studies data.

	T_G (°C)	$T_{D\ \mathrm{ONSET}}$ (°C)	T_{D50} (°C)
XL1	–48.2	305	379
XL2	–38.3	307	363
XL3	–39.5	306	399
XL4	–2.3	322	399
XL5	–34.4	302	362
XL6	–22.5	310	398
XL7	–14.8	316	386

All networks are highly homogeneous with narrow glass transitions, as measured by the full width at half maximum (FWHM) of the tan delta curve. **XL1–2**, and **XL4–7** each have FWHM of between 9 and 10 °C, whereas **XL3** has slightly higher heterogeneity with a FWHM of 16 °C (Table S1). These narrow transitions are characteristic of networks formed through the thiol-ene reaction.[34]

Conclusions

This study demonstrates the effect of the silyl R group on silyl ether networks' degradation behavior, dye release profile, and thermal properties. A series of silyl ether acrylate and thiol monomers, differing in the R groups attached to the Si atom, was synthesized through straightforward substitution reactions of alkylchlorosilanes. The networks were prepared through thiol–Michael addition reactions, utilizing a primary–amine catalyst after mixing stoichiometric equivalent amounts of acrylate and thiol monomers. A direct correlation between the steric hindrance and hydrophobicity of the monomers, and degradation and dye release were determined. Comparing the dye release behavior of degradable and non–degradable networks demonstrated that dye release is mostly under the control of degradation. The possibility of further tuning the behavior of the networks was verified by mixing different mass ratios of degradable and non–degradable monomers. As expected, the greatest mass loss and dye release were obtained from the networks possessing a higher mole ratio of degradable monomers. Thermal characterization of the networks demonstrates the possibility of carefully controlling the networks' T_g by varying the silyl R group, or by mixing different mole ratios of degradable and non–degradable monomers.

Future work may include varying the crosslink densities of the networks through the incorporation of monomers with a lesser or greater degree of functionality. This may prove to increase the understanding of release characteristics through examining the relationship between degree of functionality and degradation rate.

Acknowledgements

The SMU authors thank the W. W. Caruth, Jr. Foundation at Communities Foundation of Texas (CFT), the Retina Foundation of the Southwest, and Southern Methodist University for financial support of this work. The UT-Dallas authors thank the National Science Foundation (Grant No. 1752846) for support.

Supporting Information

ATR–FTIR spectra of networks XL1–7, HETCOR and HMBC spectra of compound DG1, GC chromatograms of degradation product and DG1, Mass spectra of degradation product and DG1.

References

(1) Lutolf, M. P.; Tirelli, N.; Cerritelli, S.; Cavalli, L.; Hubbell, J. A. Systematic Modulation of Michael-Type Reactivity of Thiols through the Use of Charged Amino Acids. *Bioconjug. Chem.* **2001**, *12*, 1051–1056.

(2) Lutolf, M. P.; Hubbell, J. A. Synthesis and Physicochemical Characterization of End-Linked Poly(Ethylene Glycol)-Co-Peptide Hydrogels Formed by Michael-Type Addition. *Biomacromolecules* **2003**, *4*, 713–722.

(3) Elbert, D. L.; Hubbell, J. A. Conjugate Addition Reactions Combined with Free-Radical Cross-Linking for the Design of Materials for Tissue Engineering. *Biomacromolecules* **2001**, *2*, 430–441.

(4) Elbert, D. L.; Pratt, A. B.; Lutolf, M. P.; Halstenberg, S.; Hubbell, J. A. Protein Delivery from Materials Formed by Self-Selective Conjugate Addition Reactions. *J. Controlled Release* **2001**, *76*, 11–25.

(5) Shieh, P.; Zhang, W.; Husted, K. E. L.; Kristufek, S. L.; Xiong, B.; Lundberg, D. J.; Lem, J.; Veysset, D.; Sun, Y.; Nelson, K. A.; Plata, D. L.; Johnson, J. A. Cleavable Comonomers Enable Degradable, Recyclable Thermoset Plastics. *Nature* **2020**, *583*, 542–547.

(6) Kunduru, K. R.; Basu, A.; Domb, A. J. Biodegradable Polymers: Medical Applications. In *Encyclopedia of Polymer Science and Technology*; John Wiley & Sons, Inc., Ed.; John Wiley & Sons, Inc.: Hoboken, NJ, USA, 2016; pp 1–22.

(7) Cooper, G. D.; Williams, B. Hydrolysis of Simple Aromatic Esters and Carbonates. *J. Org. Chem.* **1962**, *27*, 3717–3720.

(8) Patel, A.; Cholkar, K.; Agrahari, V.; Mitra, A. K. Ocular Drug Delivery Systems: An Overview. *World J. Pharmacol.* **2013**, *2*, 47–64.

(9) Yasukawa, T.; Ogura, Y.; Sakurai, E.; Tabata, Y.; Kimura, Hideya. Intraocular Sustained Drug Delivery Using Implantable Polymeric Devices. *Adv. Drug Deliv. Rev.* **2005**, *57*, 2033–2046.

(10) Mostafavi, Sa.; Karkhane, R.; Riazi-Esfahani, M.; Dorkoosh, F.; Rafiee-Tehrani, M.; Tamaddon, L. Design and Development of Intraocular Polymeric Implant Systems for Long-Term Controlled-Release of Clindamycin Phosphate for Toxoplasmic Retinochoroiditis. *Adv. Biomed. Res.* **2015**, *4*, 32.

(11) Lyu, S.; Untereker, D. Degradability of Polymers for Implantable Biomedical Devices. *Int. J. Mol. Sci.* **2009**, *10*, 4033–4065.

(12) Fu, Y.; Kao, W. J. Drug Release Kinetics and Transport Mechanisms of Non-Degradable and Degradable Polymeric Delivery Systems. *Expert Opin. Drug Deliv.* **2010**, *7*, 429–444.

(13) Parrott, M. C.; Luft, J. C.; Byrne, J. D.; Fain, J. H.; Napier, M. E.; DeSimone, J. M. Tunable Bifunctional Silyl Ether Cross-Linkers for the Design of Acid-Sensitive Biomaterials. *J. Am. Chem. Soc.* **2010**, *132*, 17928–17932.

(14) Ware, T.; Jennings, A. R.; Bassampour, Z. S.; Simon, D.; Son, D. Y.; Voit, Walter. Degradable, Silyl Ether Thiol-Ene Networks. *RSC Adv.* **2014**, *4*, 39991–40002.

(15) Sample, C. S.; Lee, S.-H.; Bates, M. W.; Ren, J. M.; Lawrence, J.; Lensch, V.; Gerbec, J. A.; Bates, C. M.; Li, S.; Hawker, C. J. Metal-Free Synthesis of Poly(Silyl Ether)s under Ambient Conditions. *Macromolecules* **2019**, *52*, 1993–1999.

(16) Shieh, P.; Nguyen, H. V.-T.; Johnson, J. A. Tailored Silyl Ether Monomers Enable Backbone-Degradable Polynorbornene-Based Linear, Bottlebrush and Star Copolymers through ROMP. *Nat. Chem.* **2019**, *11*, 1124–1132.

(17) Wang, Y.; Fan, S.; Xiao, D.; Xie, F.; Li, W.; Zhong, W.; Zhou, X. Novel Silyl Ether-Based Acid-Cleavable Antibody-MMAE Conjugates with Appropriate Stability and Efficacy. *Cancers* **2019**, *11*, 957.

(18) Kharkar, P. M.; Rehmann, M. S.; Skeens, K. M.; Maverakis, E.; Kloxin, A. M. Thiol–Ene Click Hydrogels for Therapeutic Delivery. *ACS Biomater. Sci. Eng.* **2016**, *2*, 165–179.

(19) Poetz, K. L.; Durham, O. Z.; Shipp, D. A. Thiol-X Chemistries for the Production of Degradable Polymers. In *Thiol-X Chemistries in Polymer and Materials Science*; Lowe, A., Bowman, C., Eds.; Royal Society of Chemistry: Washington, DC, 2013; pp 59–75.

(20) Hoyle, C. E.; Lowe, A. B.; Bowman, C. N. Thiol-Click Chemistry: A Multifaceted Toolbox for Small Molecule and Polymer Synthesis. *Chem. Soc. Rev.* **2010**, *39*, 1355–1387.

(21) Bañuls, M.-J.; González-Martínez, M. Á.; Sabek, J.; García-Rupérez, J.; Maquieira, Á. Thiol-Click Photochemistry for Surface Functionalization Applied to Optical Biosensing. *Anal. Chim. Acta* **2019**, *1060*, 103–113.

(22) Lowe, A. B. Thiol–Ene "Click" Reactions and Recent Applications in Polymer and Materials Synthesis: A First Update. *Polym Chem* **2014**, *5*, 4820–4870.

(23) Machado, T. O.; Sayer, C.; Araujo, P. H. H. Thiol-Ene Polymerisation: A Promising Technique to Obtain Novel Biomaterials. *Eur. Polym. J.* **2017**, *86*, 200–215.

(24) Nair, D. P.; Podgórski, M.; Chatani, S.; Gong, T.; Xi, W.; Fenoli, C. R.; Bowman, C. N. The Thiol-Michael Addition Click Reaction: A Powerful and Widely Used Tool in Materials Chemistry. *Chem. Mater.* **2014**, *26*, 724–744.

(25) Xi, W.; Scott, T. F.; Kloxin, C. J.; Bowman, C. N. Click Chemistry in Materials Science. *Adv. Funct. Mater.* **2014**, *24*, 2572–2590.

(26) Xu, Z.; Bratlie, K. M. Click Chemistry and Material Selection for *in Situ* Fabrication of Hydrogels in Tissue Engineering Applications. *ACS Biomater. Sci. Eng.* **2018**, *4*, 2276–2291.

(27) Zou, Y.; Zhang, L.; Yang, L.; Zhu, F.; Ding, M.; Lin, F.; Wang, Z.; Li, Y. "Click" Chemistry in Polymeric Scaffolds: Bioactive Materials for Tissue Engineering. *J. Controlled Release* **2018**, *273*, 160–179.

(28) Allen, C. F. H.; Fournier, J. O.; Humphlett, W. J. Thermal Reversibility of the Michael Reaction. IV. Thiol Adducts. *Can. J. Chem.* **1964**, *42*, 2616–2620.

(29) Binder, W. H.; Sachsenhofer, R. 'Click' Chemistry in Polymer and Material Science: An Update. *Macromol. Rapid Commun.* **2008**, *29*, 952–981.

(30) Binder, W. H.; Sachsenhofer, R. 'Click' Chemistry in Polymer and Materials Science. *Macromol. Rapid Commun.* **2007**, *28*, 15–54.

(31) Moses, J. E.; Moorhouse, A. D. The Growing Applications of Click Chemistry. *Chem. Soc. Rev.* **2007**, *36*, 1249–1262.

(32) Nandivada, H.; Jiang, X.; Lahann, J. Click Chemistry: Versatility and Control in the Hands of Materials Scientists. *Adv. Mater.* **2007**, *19*, 2197–2208.

(33) Kade, M. J.; Burke, D. J.; Hawker, C. J. The Power of Thiol-Ene Chemistry. *J. Polym. Sci. Part Polym. Chem.* **2010**, *48*, 743–750.

(34) Hoyle, C. E.; Bowman, C. N. Thiol-Ene Click Chemistry. *Angew. Chem. Int. Ed.* **2010**, *49*, 1540–1573.

(35) Rydholm, A. E.; Bowman, C. N.; Anseth, K. S. Degradable Thiol-Acrylate Photopolymers: Polymerization and Degradation Behavior of an in Situ Forming Biomaterial. *Biomaterials* **2005**, *26*, 4495–4506.

(36) Bounds, C. O.; Goetter, R.; Pojman, J. A.; Vandersall, Max. Preparation and Application of Microparticles Prepared via the Primary Amine-Catalyzed Michael Addition of a Trithiol to a Triacrylate. *J. Polym. Sci. Part Polym. Chem.* **2012**, *50*, 409–422.

(37) Zustiak, S. P.; Leach, J. B. Hydrolytically Degradable Poly(Ethylene Glycol) Hydrogel Scaffolds with Tunable Degradation and Mechanical Properties. *Biomacromolecules* **2010**, *11*, 1348–1357.

(38) Rizzi, S. C.; Hubbell, J. A. Recombinant Protein-Co-PEG Networks as Cell-Adhesive and Proteolytically Degradable Hydrogel Matrixes. Part I: Development and Physicochemical Characteristics. *Biomacromolecules* **2005**, *6*, 1226–1238.

(39) Jennings, A. R.; Son, D. Y. Multifunctional Thiols from the Highly Selective Reaction of Mercaptoalcohols with Chlorosilanes. *Chem. Commun. Camb. Engl.* **2013**, *49*, 3467–3469.

(40) Son, D. Y.; Jennings, A. R. Multi-Thiol Mercaptoalkoxysilane Compositions. US9243006B2, January 26, 2016.

(41) Davidson, R. S.; Ellis, R.; Tudor, S.; Wilkinson, S. A. The Photopolymerization of Acrylates and Methacrylates Containing Silicon. *Polymer* **1992**, *33*, 3031–3036.

(42) Cheng, X.; Shi, Wenfang. UV-Curing Behavior and Properties of Tri/Di(Acryloyloxyethyloxy) Phenyl Silane Used for Flame-Retardant Coatings. *Prog. Org. Coat.* **2010**, *69*, 252–259.

(43) Wang, J.; Sun, X.; Mao, W.; Sun, W.; Tang, J.; Sui, M.; Shen, Y.; Gu, Zhongwei. Tumor Redox Heterogeneity-Responsive Prodrug Nanocapsules for Cancer Chemotherapy. *Adv. Mater. Weinh. Ger.* **2013**, *25*, 3670–3676.

(44) Bhal, S. K. *LogP—Making Sense of the Value*; Advanced Chemistry Development, INC. (ACD/Labs, www.acdlabs.com); pp 1–4.

(45) Magenau, A. J. D.; Richards, J. A.; Pasquinelli, M. A.; Savin, D. A.; Mathers, R. T. Systematic Insights from Medicinal Chemistry To Discern the Nature of Polymer Hydrophobicity. *Macromolecules* **2015**, *48*, 7230–7236.

(46) Chan, J. E.; Pridgen, T. A.; Csaky, K. G. Episcleral Clearance of Sodium Fluorescein from a Bioerodible Sub-Tenon's Implant in the Rat. *Exp. Eye Res.* **2010**, *90*, 501–506.

(47) Li, G.; Guo, J.; Wang, X.; Wei, Jie. Microencapsulation of a Functional Dye and Its UV Crosslinking Controlled Releasing Behavior. *J. Polym. Sci. Part Polym. Chem.* **2009**, *47*, 3630–3639.

(48) Li, D.; Zhang, Y.; Jin, S.; Guo, J.; Gao, H.; Wang, Changchun. Development of a Redox/PH Dual Stimuli-Responsive Magnetic Supraparticle@P(Methylacrylic Acid-Co-N,N-Bis(Acryloyl)Cystamine) Drug Delivery System for Programmed Release of Anticancer Drugs in Tumor Cells. *J. Mater. Chem. B Mater. Biol. Med.* **2014**, *2*, 5187–5194.

(49) Natarajan, J.; Madras, G.; Chatterjee, Kaushik. Maltitol-Based Biodegradable Polyesters with Tailored Degradation and Controlled Release for Bone Regeneration. *RSC Adv.* **2016**, *6*, 40539–40551.

(50) Poetz, K. L.; Mohammed, H. S.; Snyder, B. L.; Liddil, G.; Samways, D. S. K.; Shipp, D. A. Photopolymerized Cross-Linked Thiol-Ene Polyanhydrides: Erosion, Release, and Toxicity Studies. *Biomacromolecules* **2014**, *15*, 2573–2582.

(51) Im, J.; Assays, C.; Mosmann, T. Rapid Colorimetric Assay for Cellular Growth and Survival: Application to Proliferation and Cytotoxicity Assays. *J. Immunol. Methods* **1983**, *65*, 55–63.

(52) Sheftel, V. O. *Indirect Food Additives and Polymers: Migration and Toxicology*; CRC Press, 2000.